3610 *Chem. Mater.* **2010,** *22,* 3610–3618
DOI:10.1021/cm903862y

CHEMISTRY OF MATERIALS
Article

Reduction-Tolerant Oxygen-Permeable Perovskite-Type Oxide $Sr_{0.7}Ba_{0.3}Fe_{0.9}Mo_{0.1}O_{3-\delta}$

Xueliang Dong, Wanqin Jin,* and Nanping Xu

State Key Laboratory of Materials-Oriented Chemical Engineering, College of Chemistry and Chemical Engineering, Nanjing University of Technology, 5 Xinmofan Road, Nanjing 210009, P. R. China

Received June 11, 2009. Revised Manuscript Received May 14, 2010

The mixed ionic-electronic conducting (MIEC) materials that have been developed for catalytic membrane reactors are vulnerable to a reducing atmosphere, especially H_2. We reported on a MIEC oxide, $Sr_{0.7}Ba_{0.3}Fe_{0.9}Mo_{0.1}O_{3-\delta}$ (SBFM), with a cubic perovskite structure ($a = 3.91$ Å at room temperature). SBFM can maintain full perovskite structure in a 5 vol % H_2/He atmosphere at 900 °C even for 50 h. The high reduce-tolerant property was mainly attributed to the synergistic effect between Mo(VI)/Mo(V) and Fe^{3+}/Fe^{2+} couples. SBFM also exhibited good tolerance to a CO_2 atmosphere at high temperature (≥900 °C) but reacted with CO_2 at relatively low temperature (< 800 °C). The introduction of Mo ion into the Fe site greatly improved the thermal stabilization of the SBFM oxide. The average thermal expansion coefficients in nitrogen atmosphere were 12.8×10^{-6} and 20.8×10^{-6} °C $^{-1}$ in the temperature ranges of 200−600 and 600−900 °C, respectively. At 900 °C, the oxygen permeation flux of SBFM membrane (1 mm in thickness) was 4.39×10^{-7} mol cm^{-2} s^{-1}. The oxygen permeation activation energy (E_a) was 42 kJ mol^{-1}, which was significantly lower than that of commonly used MIEC membranes.

1. Introduction

As a result of the potential impacts on energy, environment, and economy, mixed ionic-electronic conducting (MIEC) materials, with great oxygen ionic and electronic conductivities at high temperatures (> 700 °C), have attracted considerable interests in many promising applications, such as oxygen separation,[1,2] solid oxide fuel cells (SOFCs),[3,4] and catalytic membrane reactors.[5−8] Among these applications, the partial oxidation of light hydrocarbons in the oxygen permeable membrane reactors has important commercial benefits (for hydrogen or syngas production). Now, a big challenge for this process is that the membrane materials must be thermally and chemically stable at elevated temperature and under a reducing atmosphere (the mixture of hydrogen and carbon monoxide).[6−8] Unfortunately, few MIEC materials are able to tolerate this reducing environment.[8] Thus, in the past two decades, the development of highly stable (especially in a H_2 atmosphere) MIEC materials with considerable oxygen permeation flux has always been the common goal of all researchers in this area.

As for perovskite-related MIEC materials, the thermochemical stability mainly depends on the B site transition elements.[9] A cobalt-contained perovskite will usually be reduced in a reducing condition. Thus, the development of Co-free perovskite oxides for membrane reactor applications became the mainstream in a period of time. Sammels et al.[10] patented a series of stable $La_{2-x}Sr_xGa_yFe_{2-y}O_{5+\delta}$ MIEC materials; however, one drawback of using these materials was the low oxygen permeability. Zhu et al.[11] reported a new series of Co-free MIEC materials based on $BaCe_xFe_{1-x}O_{3-\delta}$, which can maintain the perovskite structure at 950 °C and under a 5 vol % H_2/Ar mixture gas for 1 h, whereas these materials were reduced at 900 °C under the same atmosphere for 5 h. Wang et al.[12] also reported a Co-free $Ba_{0.5}Sr_{0.5}Zn_{0.2}Fe_{0.8}O_{3-\delta}$ MIEC material, which was stable at 900 °C under a 2 vol % H_2/Ar mixture gas during the in situ XRD measurement but did not show the long-time stability under an H_2-contained atmosphere. Besides the reducing gases, a small amount of CO_2 always exists in the practical application process of a MIEC membrane. As is well-known, CO_2 is a sensitive gas to most of the MIEC materials[6,13,14] because of the existence of

*Corresponding author. E-mail: wqjin@njut.edu.cn. Tel: (+86) 25-8317-2266. Fax: (+86) 25-8317-2292.

(1) Merkle, R.; Maier, J.; Bouwmeester, H. J. M. *Angew. Chem., Int. Ed.* **2004**, *43*, 5069.
(2) Wang, H. H.; Werth, S.; Schiestel, T.; Caro, J. *Angew. Chem., Int. Ed.* **2005**, *117*, 7066.
(3) Shao, Z. P.; Sossina, M. H. *Nature* **2004**, *49*, 170.
(4) Huang, Y. H.; Dass, R. I.; Xing, Z. L.; Goodenough, J. B. *Science* **2006**, *312*, 254.
(5) Balachandran, U.; Dusek, J. T.; Maiya, P. S.; Ma, B.; Mieville, R. L.; Kleefisch, M. S.; Udovich, C. A. *Catal. Today* **1997**, *36*, 265.
(6) Jin, W. Q.; Zhang, C.; Chang, X. F.; Fan, Y. Q.; Xing, W. H.; Xu, N. P. *Environ. Sci. Technol.* **2008**, *42*, 3064.
(7) Chen, C. S.; Feng, S. J.; Ran, S.; Zhu, D. C.; Liu, W.; Bouwmeester, H. J. M. *Angew. Chem., Int. Ed.* **2003**, *42*, 5196.
(8) Bouwmeester, H. J. M. *Catal. Today* **2003**, *82*, 141.
(9) Konysheva, E.; Irvine, T. S. *Chem. Mater.* **2009**, *21*, 1514.
(10) Schwartz, M.; White, J. H.; Sammels, A. F. U.S. Patent 6214757, 2001.
(11) Zhu, X. F.; Cong, Y.; Yang, W. S. *J. Membr. Sci.* **2006**, *283*, 38.
(12) Wang, H. H.; Tablet, C.; Feldhoff, A.; Caro, J. *Adv. Mater.* **2005**, *17*, 1785.
(13) Yi, J. X.; Feng, S. J.; Zuo, Y. B.; Liu, W.; Chen, C. S. *Chem. Mater.* **2005**, *17*, 5856.
(14) Yan, A. Y.; Yang, M.; Hou, Z. F.; Dong, Y. L.; Cheng., M. J. *J. Power Sources* **2008**, *185*, 76.

Published on Web 05/25/2010

alkaline-earth elements in these materials. Therefore, in addition to the high stability in the reducing atmosphere, the considerable CO_2-tolerated property is also important for the application of MIEC materials.

$SrFeO_{3-\delta}$-based perovskite oxides exhibit a considerable level of oxygen permeability and phase stability.[15,16] Moreover, the performances of these materials can be further improved by ion substitution in A and/or B sites.[15,16] Recently, Huang and Goodenough et al., reported a series of Mo-based double-perovskite anode materials for SOFCs, such as $Sr_2Mg_{1-x}Mn_xMoO_{6-\delta}$, Sr_2MMoO_6 (M = Co, Ni),[17] and La-doped $Sr_2MgMoO_{6-\delta}$[18] oxides. Most of these oxides showed an extremely stable performance in a reducing fuel atmosphere (containing H_2, CH_4, and CO, etc.). Even more surprising, Sr_2CoMoO_6 oxide can maintain full structure after being treated in 5 vol % H_2/Ar at 800 °C for 20 h, and the fraction of impurity phase was too small to be detected. Moreover, the valence of Mo cation was nearly the same as that in MoO_3, indicating that Mo was predominantly in VI valence. Rager et al.[19] studied the phase diagram of a $SrO-Fe_3O_4-MoO_3$ system under 1 vol % H_2/Ar at 1200 °C and stated that Mo^{5+} and Mo^{6+} were present in $Sr_2Fe_{2-x}Mo_xO_y$. Wang et al.[20] reported that a high-quality Sr_2FeMoO_6 film can be prepared by pulsed laser deposition in a 10 vol % H_2/Ar atmosphere at different temperatures (from 700−900 °C). All of these examples show high stability of Mo cation and Mo-based oxides in a reducing atmosphere; therefore, we think that it is possible to replace a desired fraction of Fe in $SrFeO_{3-\delta}$-based oxides with Mo to form a solid solution that exhibits both adequate oxygen permeability and sufficient phase stability.

Here, we report the evaluation of a new type of $Sr_{0.7}Ba_{0.3}Fe_{1-x}Mo_xO_{3-\delta}$ perovskite oxide, where iron and molybdenum are all present on the octahedral B site. This produces the cubic composite $Sr_{0.7}Ba_{0.3}Fe_{0.9}Mo_{0.1}O_{3-\delta}$ (SBFM) with a Mo doping as a new MIEC material. SBFM shows the highest chemical stability (in a 5 vol % H_2/He atmosphere and at high temperature) in all known perovskite-based oxygen permeable materials and promising oxygen permeability.

2. Experimental Section

2.1. Preparation of SBFM Samples. SBFM powders were synthesized via a combined ethylenediaminetetraacetic acid (EDTA)−citrate complexing sol−gel process with Sr, Ba and Fe metal nitrates and MoO_3 (dissolved in $NH_3 \cdot H_2O$ first). Stoichiometric amounts of nitrates were mixed into a measured volume of deionized water under continuous agitation. The necessary amount of EDTA, dissolved in NH_3 solution, was then dropped to the mixed metal nitrate solution, followed by the addition of solid citric acid with stirring (mole ratio of total metal ions to EDTA and to citrate = 1:1:2). The oxidant fuel ratio and the pH of the precursor were adjusted to desired values using nitric acid and ammonium hydroxide. The solution containing the complex precursor was then heated on a hot plate at 250 °C for about 5 h to produce a black, soft, and fluffy product. Finally, the products were calcined in air at 950 °C for 5−10 h to prepare SBFM oxide. The calcined powders were uniaxially pressed at 400 MPa, and the green disk membranes (16 mm in diameter) were sintered at 1250 °C for 10 h in stagnant air with a heating and cooling rate of 2 °C min^{-1}. The actual densities of the sintered membranes exceeded 95% of the theoretical densities in all cases. Synthesis of other compounds, $BaCe_{0.15}Fe_{0.85}O_{3-\delta}$ (BCF) and $La_{0.6}Sr_{0.4}Co_{0.2}Fe_{0.8}O_{3-\delta}$ (LSCF), followed the same route. All samples were calcined in air at 950 °C for 5−10 h to achieve full crystal structures and sintered at 1200 °C for 5−10 h to get dense bodies.

2.2. Characterization. The crystal structures of the samples were characterized by X-ray diffraction (XRD, D8-advance, Bruker, Germany) using Cu Kα radiation. The experimental diffraction patterns were collected at room temperature by step scanning in the range of $20° \leq 2\theta \leq 80°$. The elemental compositions of SBFM powders and membranes were analyzed by inductively coupled plasma optical emission spectrometry (ICP-OES, PE Optima 2000DV, PerkinElmer, USA). The microstructures of the SBFM samples were analyzed by a high-resolution transmission electron microscope (TEM, JEM-2010 UHR, Japan). Prior to the TEM measurements, the sintered membrane was crushed in an agate mortar, ultrasonically dispersed in ethanol, and collected with 300 mesh copper-supported perforated carbon foil. The thermogravimetry and differential scanning calorimetry (TG-DSC) (STA 409 PC, Netzsch, Germany) analysis of SBFM samples (SBFM membrane was crushed and ground to be powder for the TG-DSC test) was performed in the range of 25−900 °C with a heating rate of 5 °C min^{-1} in N_2 and 5 vol % H_2/N_2 and CO_2 atmospheres, respectively. Then, the oxygen nonstoichiometry (δ) of the sample was calculated based on the TG-DSC data.[21] The initial oxygen nonstoichiometry (δ_o) of the sample was estimated by an iodometric titration experiment (see Supporting Information).[22] The electrical conductivities of the sintered samples were measured in helium (He) by a four-probe DC instrument (2440 5A, Keithley, USA), where the Ag paste and Ag wire were used to connect the sample and instrument. The surface chemical composition of the SBFM powders was analyzed by X-ray photoelectron spectra (XPS, Thermo ESCALAB 250, USA), equipped with an Al Kα X-ray source ($h\nu$ = 1486.6 eV). All binding energies (BE) were referenced to the adventitious C 1s line at 284.6 eV. The thermal expansion behaviors of the samples were investigated by a dilatometry (Netzsch DIL 402C, Germany) in nitrogen to 900 °C at a heating rate of 5 °C min^{-1}. The samples were sintered at 1250 °C for 10 h in stagnant air before the test.

2.3. Chemical Stability Measurements. SBFM powder samples were calcined at 950 °C for 10 h and then annealed at different temperatures for various times in 5 vol % H_2/He (with an oxygen partial pressure of $\sim 1 \times 10^{-7}$ Pa), 20 vol % CO_2/He (with an oxygen partial pressure of ~10 Pa), or pure CO_2. The samples were cooled down rapidly to room temperature under

(15) Kharton, V. V.; Shaula, A. L.; Snijkers, F. M. M.; Cooymans, J. F. C.; Luyten, J. J.; Yaremchenko, A. A.; Valente, A. A.; Tsipis, E. V.; Frade, J. R.; Marques, F. M. B.; Rocha, J. *J. Membr. Sci.* **2005**, *252*, 215.
(16) Teraoka, Y.; Shimokawa, H.; Kang, C. Y.; Kusaba, H.; Sasaki, K. *Solid State Ionics* **2006**, *177*, 2245.
(17) Huang, Y. H.; Liang, G.; Croft, M.; Lehtimaki, M.; Karppinen, M.; Goodenough, J. B. *Chem. Mater.* **2009**, *21*, 2319.
(18) Ji, Y.; Huang, Y. H.; Ying, J. R.; Goodenough, J. B. *Electrochem. Commun.* **2007**, *9*, 1881.
(19) Rager, J.; Zipperle, M.; Sharma, A.; MacManus-Deiscoll, J. L. *J. Am. Ceram. Soc.* **2004**, *87*, 1330.
(20) Wang, S. Q.; Pan, H. Y.; Zhang, X. P.; Lian, G. J.; Xiong, G. C. *Appl. Phys. Lett.* **2006**, *88*, 121912.
(21) Dong, X. L.; Xu, Z.; Chang, X. F.; Zhang, C.; Jin, W. Q. *J. Am. Ceram. Soc.* **2007**, *90*, 3923.
(22) Chang, X. F.; Zhang, C.; Dong, X. L.; Zhou, W.; Jin, W. Q.; Shao, Z. P.; Xu, N. P. J. *J. Membr. Sci.* **2008**, *316*, 128.

the same atmospheres, and then, the XRD patterns were taken for the treated powder samples.

2.4. Oxygen Permeation Measurements. The oxygen permeation measurement was performed on a high temperature oxygen permeation apparatus, which has been described in our previous work.[23] Air was introduced to the feed side at the flow rate of 120 mL min^{-1}, and He was used as the sweeping gas in the permeation side. The oxygen partial pressure of the permeation side was controlled to be about 200 Pa by regulating the He flow rate at the range of 20−100 mL min^{-1}. Compared with the oxygen permeation rate, the He flow rate at the permeation side was so high that the oxygen partial pressure at the membrane surface could be assumed to be identical to that measured by the gas chromatograph. The effluent streams were analyzed by online gas chromatographs (Shimadzu Model GC-8A, Japan). An internal standard gas CH_4 (about 1.0 mL min^{-1}) was added into the effluent streams and passed through the online analysis loop. The chromatograph was operated under a current of 180 mA and the attenuation of 1, conditions under which a trace amount of oxygen (> 1 Pa) could be detected.

2.5. Details of DFT Simulations. The crystal structure of SBFM was constructed based on the geometric configuration of $BaTiO_3$ perovskite oxide by a random doping method (70 at % Sr was doped into the Ba site of the $BaTiO_3$, and the Ti site was completely substituted by Fe and Mo in the ratio of 9:1). For comparison, the structural and electronic properties of $Sr_{0.7}Ba_{0.3}FeO_{3-\delta}$ (SBF) were also calculated.

All atoms in the unit cell are unconstrained and allowed to relax and reach their ground state during geometry optimization. The Perdew-Burke-Ernzerhof functional (PBE) of gradient-corrected functional was chosen as the exchange-correlation functional. The Kohn−Sham one-electron states were expanded in a plane wave basis set up to 245 eV. The Monkhorst-Pack k-points for the accuracy of the Brillouin zone sampling were set at fine level (6 × 6 × 6). Ultrasoft pseudopotential was used to perform with the lowest possible cutoff energy for the plane-wave basis set, and the space was the reciprocal space. The convergence criteria for structure optimization and energy calculation were set to the following: (a) self-consistent field (SCF) tolerance of 5.0×10^{-7} eV $atom^{-1}$; (b) energy tolerance of 5×10^{-6} eV $atom^{-1}$; (c) displacement tolerance of 5.0×10^{-4} Å; (d) force tolerance of 0.01 eV $Å^{-1}$.

3. Results and Discussion

3.1. Crystal Structure Analysis. The X-ray diffraction (XRD) pattern (Figure 1a) of the SBFM membrane sintered at 1250 °C for 10 h showed that SBFM oxide was of the cubic perovskite structure with the lattice parameter of a = 3.91 Å. The high-resolution transmission electron microscopy (HRTEM) analysis further supported this result. The HRTEM image of SBFM oxide in the [001] direction is illustrated in Figure 1b. According to the PDF card (40-0905), data of strontium iron perovskite oxide, we can find that the lattice plane distances of d_1 = 2.76 Å and d_2= 3.90 Å correspond to (110) and (010) lattice planes, respectively. Therefore, the lattice parameter can be calculated as $a = (2)^{1/2} d_{(110)} = d_{(010)}$ = 3.90 Å. Figure 1c shows the selected-area electron diffraction (SAED) pattern of SBFM oxide in the [001] zone axis.

(23) Li, S. G.; Jin, W. Q.; Huang, P.; Xu, N. P.; Shi, J.; Hu, M. Z. C.; Payzant, E. A.; Ma, Y. H. *AIChE J.* **1999**, *45*, 276.

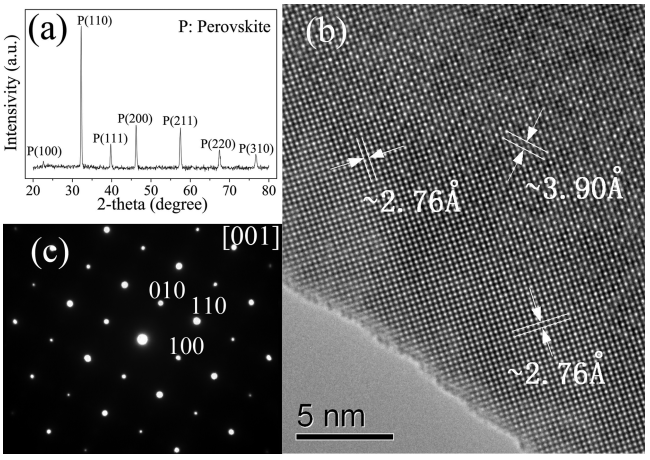

Figure 1. (a) XRD pattern of SBFM membrane sintered at 1250 °C for 10 h. (b) The HRTEM image of SBFM oxide viewed down the [001] direction. (c) The selected-area electron diffraction (SAED) pattern of SBFM oxide in the [001] zone axis.

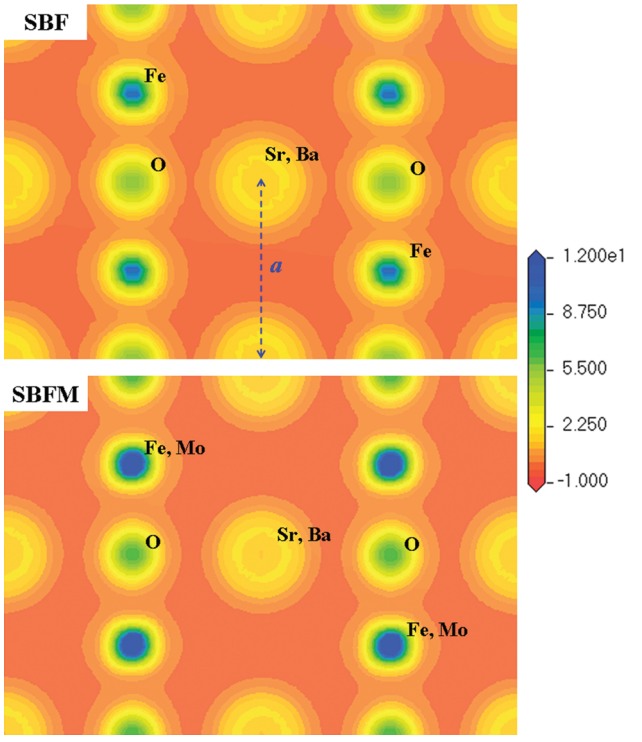

Figure 2. Electron density maps of the (110) plane of SBF and SBFM oxides.

The SAED pattern was indexed according to a cubic or tetragonal until cell. Then, the lattice plane distances can be measured by the inverse fast Fourier transform (FFT). The results were $d_{(010)}$ = 3.90 Å and $d_{(110)}$ = 2.76 Å, which were in agreement with the XRD data.

3.2. DFT Simulation. The crystal structure and electronic properties of SBFM oxide was simulated at the level of density function theory (DFT) by the Cambridge sequential total energy package (CASTEP). From the simulated crystal structure of SBF and SBFM oxides, cubic unit cells with the lattice parameter a = 3.83 and 3.88 Å, respectively, were obtained. Figures 2 shows the calculated electron density maps at the (110) plane of SBF and SBFM oxides. The high electron density region

nearby B site cations can be observed clearly in both SBF and SBFM crystals. Moreover, an obvious linear connection of electron clouds between B site cations and O can be seen, which is caused by the hybridization of O 2p orbital and Fe 3d/Mo 4d orbital. This electron cloud configuration provides the possible electron transport channel, and it is consistent with the widely accepted electronic conduction mechanism in perovskite oxide, which states that the electronic conduction is created by a B^{n+} cation capturing an electron from a neighboring $B^{(n-1)+}$ cation. However, the $B^{(n-1)+}$ cations are sufficiently far apart as to have no appreciable overlapping. Therefore, the hopping transport of charge carriers between two neighboring B cations in the perovskite lattice is mediated by the O 2p orbital as follows:[24]

$$B^{n+} - O^{2-} - B^{(n-1)+} \rightarrow B^{(n-1)+} - O^{-} - B^{(n-1)+} \rightarrow B^{(n-1)+} - O^{2-} - B^{n+} \quad (1)$$

which is known as double exchange, first discussed qualitatively by Zener.[25] This process is favored by a strong overlap of empty or partly filled cation orbitals of the *d* manifold with the filled O 2p orbital of neighboring anions. Compared with SBF, the overlap of electron clouds between B site cations and O is reduced in SBFM, which may be attributed to 2-fold. On the one hand, the Mo cation with high oxidation state in SBFM shows strong attraction for the electrons around it. The electron density of SBFM nearby the B site is obviously higher than that of SBF. The electron cloud area of the B site is also reduced by Mo cation. On the other hand, the lattice parameter increases with the introduction of Mo cation. Therefore, the doping of Mo into the Fe site may induce the decrease of electronic conductivity.

Figure 3a,b shows the calculated electronic band structures of SBF and SBFM oxides (the spin-up electronic band structure was chosen), respectively. For SBF, some valence band (VB) states go across the Fermi level and intrude upward into the lower part of the band gap. A state in the conduction bang (CB) is remarkably lowered. The top of VB is located at *R* point, and the direct energy gap is ~0.91 eV, indicating that SBFM has semiconductor features. The small energy gap means that the electron in VB is easy to be excited into the CB. In contrast, the band structures of SBFM are similar with that of SBF, only the states near fermi level change a little. However, the band gap is obviously expanded, and the direct energy gap of SBFM is ~2.61 eV, indicating semiconductor features. The effect of Mo cation on energy band structure is in good agreement with the electron density results.

3.3. Thermal and Chemical Stability Analysis. From the ICP-OES results (see Table S1 in the Supporting Information), the element compositions of SBFM powders and membranes were close to the theoretical compositions.

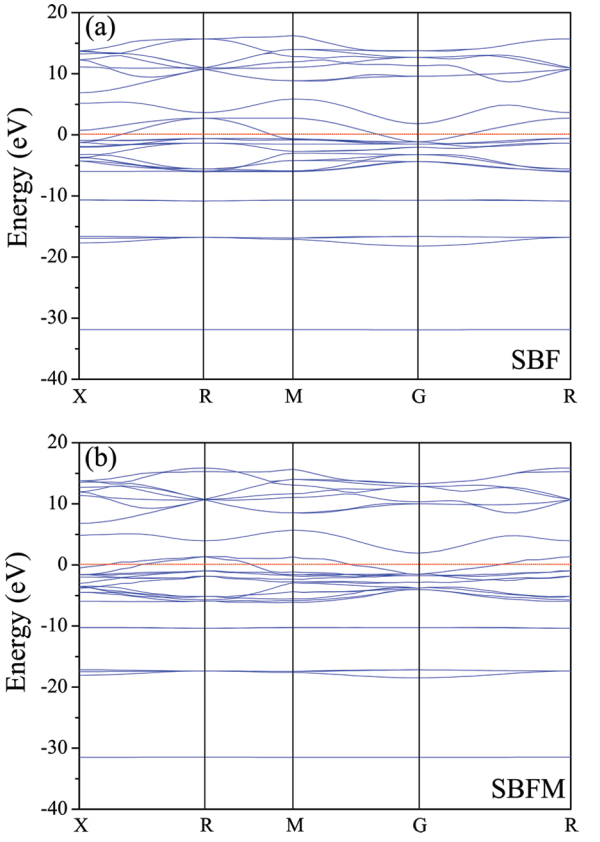

Figure 3. Calculated energy band structures of (a) SBF and (b) SBFM oxides (the spin-up energy band structure was chosen).

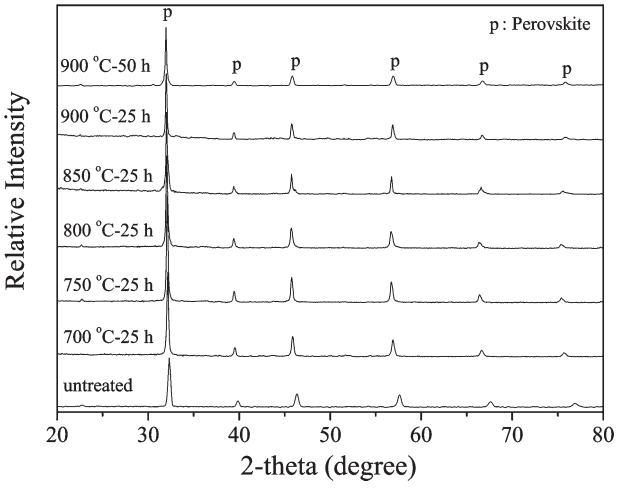

Figure 4. XRD patterns of SBFM powders calcined at 950 °C for 10 h, followed by annealing in a 5 vol % H_2/He atmosphere at different temperatures for 25 or 50 h.

Only a light decrease of Mo content in SBFM membrane (1.7%) was observed.

To evaluate the chemical stability, we exposed SBFM powder samples to 5 vol % H_2/He at different temperatures (from 700 to 900 °C) for 25 or 50 h. As shown in Figure 4, after being treated at various temperatures for 25 h or even 50 h, SBFM oxide still maintained full perovskite structure and no obvious new phases were produced. This demonstrated that SBFM oxide possessed a high chemical stability at high temperature and under

(24) Bouwmeester, H. J. M.; Burggraaf, A. J. Dense ceramic membranes for oxygen separation. In *Fundamentals of Inorganic Membrane Science and Technology*; Burggraaf, A. J.; Cot, L., Eds.; Elsevier Science B.V.: Amsterdam, 1996.
(25) Zener, C. *Phys. Rev.* **1951**, *82*, 403.

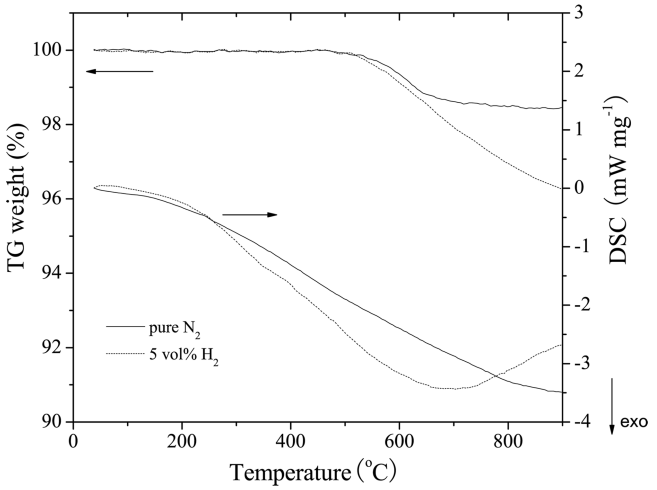

Figure 5. TG-DSC curves of SBFM oxide in N_2 and 5 vol % H_2/N_2 atmospheres with a heating rate of 5 °C min^{-1}. SBFM membrane was crushed and ground to be powder for the TG-DSC test.

a H_2 (5 vol %) atmosphere. In fact, the stability of SBFM in the H_2-contained atmosphere represents the highest one ever reported for any known perovskite-based oxygen permeable materials. The high chemical stability of SBFM oxide was further supported by the TG-DSC results, as shown in Figure 5. The onset weight loss temperature is about 500 °C in both N_2 and 5 vol % H_2/N_2 atmospheres. On heating in N_2, the weight loss mainly occurred in the temperature range of 500−700 °C, whereas a continuous weight loss was observed in H_2 above 500 °C. From room temperature to 900 °C, the total weight losses of SBFM are 1.57% and 3.95% in N_2 and H_2 (5 vol %) atmospheres, respectively. From DSC curves, no obvious endothermic or exothermic peaks can be observed.

As for the high reduce-tolerant property of SBFM oxide, one reasonable explanation is that the introduction of high valence state Mo cation into the Fe site decreases the average valence of Fe cation, especially the concentration of Fe^{4+}, which is easy to be reduced in a reducing atmosphere. In addition, Goodenough et al.[26] reported that the Mo(VI)/Mo(V) redox band overlapped the Fe^{3+}/Fe^{2+} couple in Sr_2FeMoO_6 oxide. The Fe^{3+}/Fe^{2+} couple was at a high enough energy that even in a reducing atmosphere it was not possible to reduce all the Fe^{3+} ions completely to Fe^{2+}, and the Mo(VI)/Mo(V) redox couple could be expected to remain mixed-valence in the reducing atmosphere. This statement may be a key explanation to the high chemical stability of SBFM. In order to confirm the reliability of this explanation, the X-ray photoelectron spectroscopy (XPS) was used to analyze the valence of Mo and Fe elements in SBFM oxide before and after being annealed in the 5 vol % H_2/He atmosphere. The XPS data were analyzed by the XPS peak fitting program (XPSPeak 4.1) to separate the contribution of different valences. The detailed fitting parameters of all peaks are listed in Table S2 (see Supporting Information). Figure 6a shows the Fe 2p XPS spectra. The peaks at the

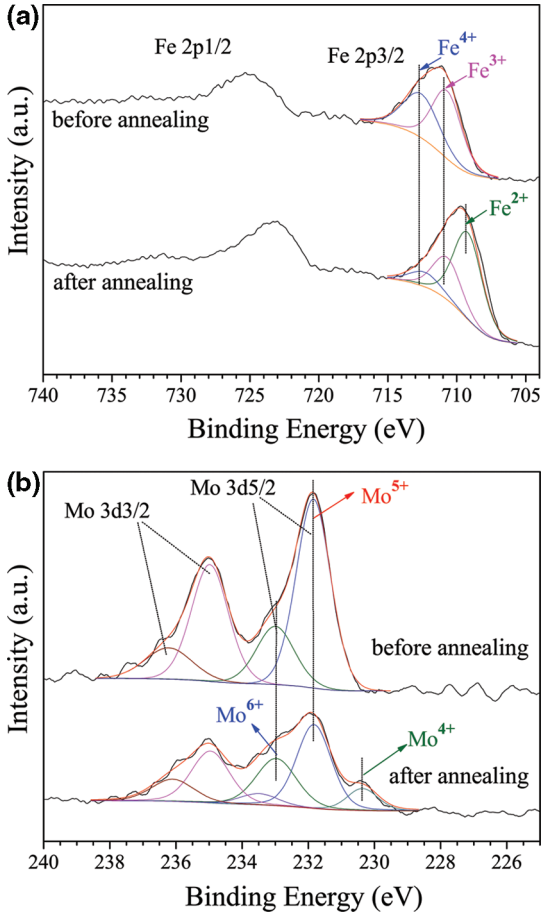

Figure 6. X-ray photoelectron spectra of the Fe 2p peaks (a) and Mo 3d peaks (b) of SBFM powders before and after being annealed in a 5 vol % H_2/He atmosphere at 900 °C for 50 h.

bonding energies of ~709.2 eV and ~710.7 eV are assigned to $Fe^{2+}2p_{3/2}$ and $Fe^{3+}2p_{3/2}$, respectively.[27] The peak at ~712.4 eV may be attributed to a higher oxidation state of Fe, which is considered to be Fe^{4+} in SBFM. Before being annealed in a H_2 (5 vol %) atmosphere, the valence of Fe ion is not lower than 3. In contrast, the coexistence of Fe^{2+}, Fe^{3+}, and Fe^{4+} peaks is observed in the annealed sample. Similar results were reported by Singh et al.[28] in $Co_{0.3}Fe_{0.7}$-$Sr_2YCu_2O_{7+\delta}$ oxide. However, the peak at ~712.3 eV in Fe 2p core level was assigned to a satellite peak. In addition, no metal Fe line at ~706.8 eV[27] can be found. Figure 5b shows the Mo 3d XPS spectra. The peaks with the bonding energy of ~232.8, ~231.7, and ~230.9 eV are associated with Mo^{6+}-$3d_{5/2}$, $Mo^{5+}3d_{5/2}$, and $Mo^{4+}3d_{5/2}$ components, respectively.[29] Mo^{6+} and Mo^{5+} existed in SBFM oxide not only before but also after being annealed in the H_2 (5 vol %) atmosphere. The Mo^{4+} peak can be fitted in the reduced sample. The XPS results presented the evidence that the high reduce-tolerant property of SBFM oxide was associated with the synergistic effect between Mo(VI)/Mo(V) and Fe^{3+}/Fe^{2+} couples.

(26) Goodenough, J. B.; Huang, Y. H. *J. Power Sources* **2007**, *173*, 1.
(27) Wagner, C. D.; Riggs, W. M.; Davis, L. E.; Moulder, J. F.; Mullenberg, G. E. *Handbook of X-Ray Photoelectron Spectroscopy*; Perkin-Elmer Corporation: Minnesota, USA, 1979.
(28) Singh, S. K.; Kumar, P.; Husain, M.; Kishan, H.; Awana, V. P. S. *J. Appl. Phys.* **2010**, *107*, 063905.
(29) Guan, J. Q.; Wu, S. J.; Wang, H. S.; Jing, S. B.; Wang, G. J.; Zhen, K. J.; Kan, Q. B. *J. Catal.* **2007**, *251*, 354.

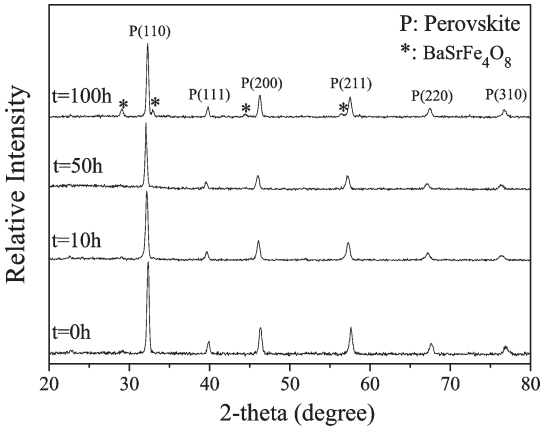

Figure 7. XRD patterns of SBFM powders calcined at 900 °C for 10 h, followed by annealing in 20 vol % CO_2/He at 900 °C for various times.

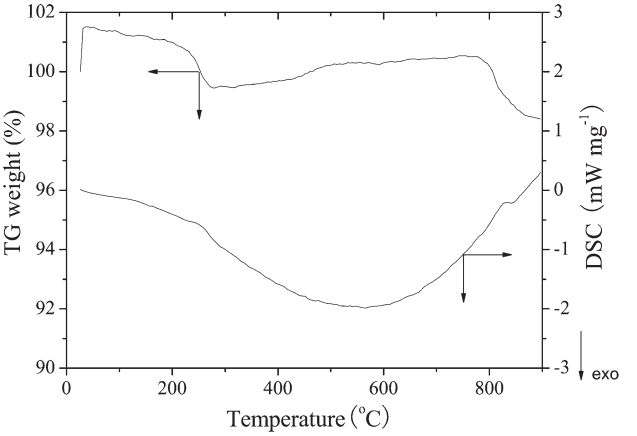

Figure 8. TG-DSC curves of SBFM oxide measured at a heating rate of 5 °C min^{-1} in a pure CO_2 atmosphere. SBFM membrane was crushed and ground to be powder for the TG-DSC test.

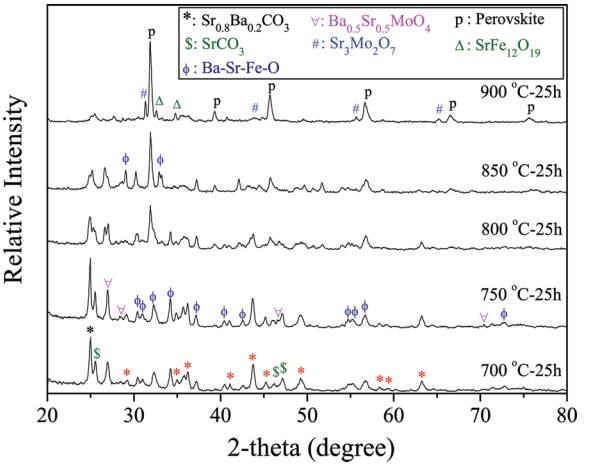

Figure 9. XRD patterns of SBFM powders calcined at 950 °C for 10 h, followed by annealing in a pure CO_2 atmosphere at different temperatures for 25 h.

On the basis of the XPS data, the valence composition of Fe and Mo elements can be estimated (see Table S3 in the Supporting Information). Then, according to the metal ions radius,[30] the tolerance factors of SBFM oxide before and after being treated in H_2 can be calculated to be 0.994 and 0.953, respectively. In general, the perovskite structure (ABO_3) can be retained as the tolerance factors are kept in the range of 0.75−1.0. Morever, the ideal cubic perovskite structure appears for a tolerance factor very close to 1.[31] Therefore, from the tolerance factor theory, the perovskite structure of SBFM oxide is very stable. From the valence composition data in Table S3 (Supporting Information), the oxygen nonstoichiometry of the as-prepared SBFM powder at room temperature can be calculated as 0.18. However, this value was determined to be 0.11 ± 0.01 by the iodometric titration experiments. This difference may be attributed to the XPS peak fitting process. Like any other mathematic fitting process of a set of nonlinear equations, the results of fitting may vary significantly with different sets of initial preset values of the parameters, such as the full width at half-maximum (FWHM), the % Gaussian−Lorentzian value, the peak position, and the peak area. Maschhoff et al.[32] found that small changes in FWHM values assigned to Fe^{2+} and Fe^{3+} component spectra resulted in significant variations in calculated Fe^{2+}/Fe^{3+} relative concentrations. Therefore, the iodometric titration results are reliable, and the fitting results can be considered as a reference.

Besides the hydrogen-contained atmosphere, the chemical stability of SBFM in the CO_2 atmosphere was also investigated. SBFM powder was annealed in the 20 vol % CO_2/He atmosphere at 900 °C. As shown in Figure 7, SBFM could keep its perovskite structure even for 100 h in 20 vol % CO_2/He at 900 °C, although a trace of $BrSrFe_4O_8$ phase could be observed. Meantime, the TG-DSC data of SBFM oxide in the pure CO_2 atmosphere was analyzed from room temperature to 900 °C. As shown in Figure 8, before 280 °C, the weight of the sample increased first and then decreased, accompanied by a small endothermic peak at about 280 °C on the DSC curve. This may be attributed to the adsorption and desorption of CO_2 on the surface of the sample at low temperature. Subsequently, the TG curve showed an almost linear weight increase from 280 to 780 °C. This process was caused by the reaction between CO_2 and the sample to produce carbonates. However, the weight of the sample decreased rapidly at high temperature (> 780 °C), and a small endothermic peak could be observed on the DSC curve at about 830 °C. This process suggested the possible decomposition of the carbonates at high temperature.

In order to get a deeper recognition to the chemical stability of SBFM oxide in the CO_2 atmosphere, the crystal structures of the sample treated in a pure CO_2 atmosphere at different temperatures for 25 h were analyzed. As shown in Figure 9, after being treated at 700 and 750 °C, the perovskite structure of SBFM oxide was totally destroyed and the characteristic peaks of strontium and/or barium carbonates could be observed. However, the strengths of these characteristic peaks gradually decreased from 800 to 900 °C. After being treated at 900 °C, the sample showed perovskite main phase and a

(30) Shannon, R. D. *Acta Crystallogr.* **1976**, *A32*, 751.
(31) Pena, M. A.; Fierro, J. L. G. *Chem. Rev.* **2001**, *101*, 1981.
(32) Maschhoff, B. L.; Armstrong, N. R. *Langmuir* **1991**, *7*, 693.

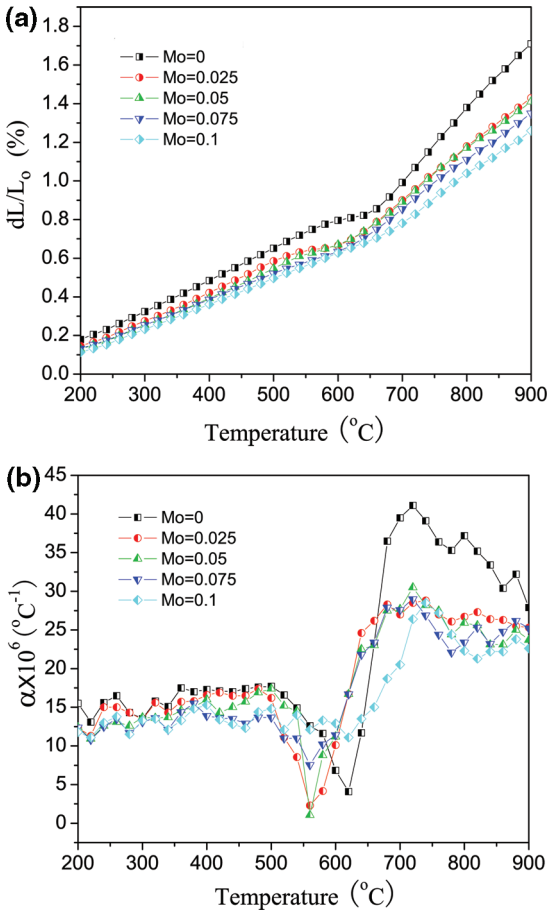

Figure 10. Thermal expansion behaviors (a) and thermal expansion coefficients (b) of $Sr_{0.7}Ba_{0.3}Fe_{1-x}Mo_xO_{3-\delta}$ (x = 0, 0.025, 0.05, 0.075, and 0.1) samples in a N_2 atmosphere. The samples were sintered at 1250 °C for 10 h in stagnant air before the test.

small amount of impurity phases. These results are in good agreement with the TG-DSC data. From Figures 7 to 9, we can found that the crystal structure of SBFM oxide was not so stable in high concentration CO_2, especially at a relatively low temperature (< 800 °C). However, compared with the Ba containing MIEC materials reported in the literature,[14,33,34] SBFM oxide showed better chemical stability in the CO_2 atmosphere.

The thermal and chemical expansion behaviors are of particular interest for the industrial application of mixed-conducting membranes because the chemical expansion on the low oxygen partial pressure side of the membrane relative to the air side can lead to a large mechanical stress across the membrane. Figure 10 shows the thermal expansion behaviors of $Sr_{0.7}Ba_{0.3}Fe_{1-x}Mo_xO_{3-\delta}$ (x = 0, 0.025, 0.05, 0.075, and 0.1) samples in a N_2 atmosphere with a heating rate of 5 °C min^{-1}. The possible effect of heating rate on the equilibrium (the oxygen exchange equilibrium between sample and gas phase) was analyzed by a comparative experiment, in which the thermal expansion behaviors of SBFM at different heating rates (3 and 5 °C min^{-1}) were tested. From the experimental results (see Figure S1 in the Supporting Information), two thermal expansion curves were almost in a superposition, and only a little difference could be observed on the thermal expansion coefficient curves. Kharton et al.[35] stated that a heating rate of 3 °C min^{-1} in the dilatometric experiments was small enough to provide equilibration.

As shown in Figure 10a, the expansion curves exhibited inflections between the temperatures of 550 and 650 °C, depending on the composites of the samples. The degree of expansion decreased with increasing amount of Mo. The nonlinear expansion behaviors of $Sr_{0.7}Ba_{0.3}Fe_{1-x}Mo_xO_{3-\delta}$ oxides were mainly caused by the loss of lattice oxygen,[36−38] which was attributed to the reduction of high valence transition-metal cations in these oxides to lower valence states at high temperatures and under low oxygen partial pressures. This expansion behavior was considered as the chemical induced expansion.[36] From Figure 10a, the chemical expansion of SBFM was the lowest. Figure 10b shows the thermal expansion coefficients (TECs) of $Sr_{0.7}Ba_{0.3}Fe_{1-x}Mo_xO_{3-\delta}$ samples in a N_2 atmosphere. It can be found that the TECs also demonstrated abrupt peaks between the temperature of 550 and 650 °C, depending on the composites of the samples. At a certain temperature, the TECs decreased with increasing amount of Mo. The average TECs of SBFM oxide in a nitrogen atmosphere are 12.8×10^{-6} and 20.8×10^{-6} °C^{-1} in the temperature ranges of 200−600 and 600−900 °C, respectively. These results indicated that Mo was a benefit for the improvement of the thermal stabilization of the SBFM oxide. However, the chemical expansion of SBFM is still an important problem that needs to be overcome before its engineering application, though it is greatly reduced by the Mo cation.

3.4. Oxygen Permeation Analysis. As for a symmetric MIEC membrane, in general, the membrane is thick enough and bulk diffusion is always the rate control step of oxygen permeation. Thus, the permeation flux can be expressed by the following equation:[39]

$$J_{O_2} = -\frac{RT}{4^2F^2L}\cdot\int_{\ln P'_{O_2}}^{\ln P''_{O_2}}\frac{\sigma_{ion}\cdot\sigma_e}{\sigma_{ion}+\sigma_e}\cdot d[\ln P_{O_2}] \qquad (2)$$

where P''_{O_2} and P'_{O_2} are the oxygen partial pressures at the feed side and sweep side membrane surface, respectively. σ_{ion} and σ_e are the oxygen ionic and electronic conductivity, respectively. L is the thickness of the membrane. Equation 2 illustrates that the permeation flux is determined by both the oxygen ionic and electronic conductivities, which reflect the transporting ability of oxygen ion and electron in this material.

To evaluate the electronic conductivity, the total electrical conductivity of sintered SBFM sample was measured by the

(33) Tong, J. H.; Yang, W. S.; Zhu, B. C.; Cai, R. *J. Membr. Sci.* **2002**, *203*, 175.
(34) Arnold, M.; Wang, H. H.; Feldhoff, A. *J. Membr. Sci.* **2007**, *293*, 44.
(35) Kharton, V. V.; Yaremchenko, A. A.; Patrakeev, M. V.; Naumovich, E. N.; Marques, F. M. B. J. *Eur. Ceram. Soc.* **2003**, *23*, 1417.
(36) Adler, S. B. *J. Am. Ceram. Soc.* **2001**, *84*, 2117.
(37) Park, C. Y.; Jacobson, A. J. *Solid State Ionics* **2005**, *176*, 2671.
(38) McIntosh, S.; Vente, J. F.; Haije, W. G.; Blank, D. H. A.; Bouwmeester, H. J. M. *Chem. Mater.* **2006**, *18*, 2187.
(39) Wanger, C. *Prog. Solid State Chem.* **1975**, *10*, 3.

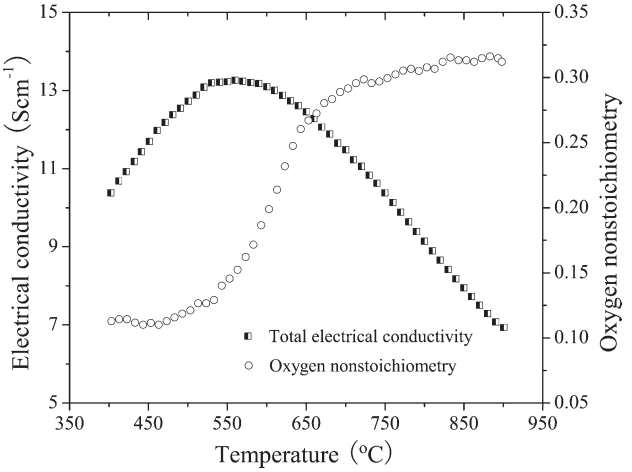

Figure 11. Temperature dependence of electrical conductivity and oxygen nonstoichiometry of SBFM samples. Electrical conductivity was measured in a He atmosphere based on the samples sintered at 1250 °C for 10 h in stagnant air. Oxygen nonstoichiometry was estimated from the TG data.

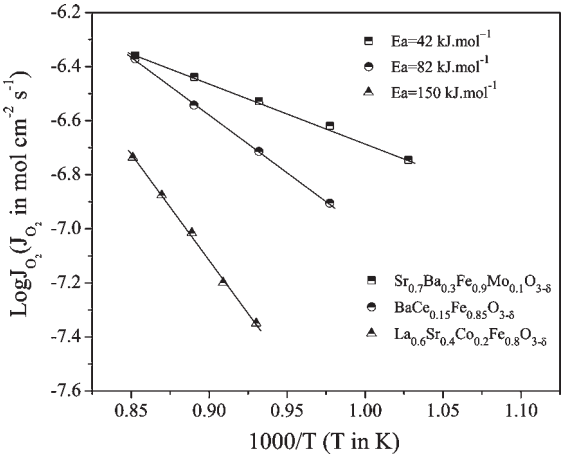

Figure 12. Aerrhenius plots of oxygen permeation fluxes through SBFM, BCF, and LSCF membranes. The thickness of each membrane is 1.0 mm. The oxygen partial pressure gradient across the membrane is about 2.1 × 10^4 Pa/200 Pa.

four-probe DC method under He atmosphere in the temperature range of 400−900 °C. At each temperature point, the data were not recorded until the samples have reached the equilibrium with the gas phase around the samples. The result is shown in Figure 11. Since the oxygen ionic conductivity is much lower than the electronic conductivity in SBFM, the measured value approximately refers to the electronic conductivity alone. SBFM showed the semiconductor behavior at the relatively low temperature, characterized by the increase of the conductivity with the increase of temperature, until it reached a maximum value of ∼13.3 S cm^{-1} at about 560 °C. With the further increase of temperature, the electrical conduction started to show the metal-like behavior, i.e., the decrease of the electrical conductivity with the increase of temperature, which was caused by the hopping of small polarons associated with the low valence states of the B site ions. The release of oxygen from the SBFM lattice at high temperature and under low oxygen partial pressure changed the relative concentrations of various valence states of B site ions and, therefore, affected the electronic conductivity. The transition of electrical conductivity behavior (from semiconductor to metal-like) with increasing the temperature is consistent with the DFT calculated result (the small energy gap of SBFM oxide facilitates electron transition from VB into CB). The oxygen ionic conductivity of the SBFM sample can be analyzed indirectly according to the oxygen nonstoichiometry value. The oxygen nonstoichiometry of SBFM in the N_2 atmosphere was estimated from the TG and iodometric titration data, and the result was also illustrated in Figure 11. The oxygen nonstoichiometry increases with increasing the temperature. It increases rapidly from 500 to 600 °C and then trends to a constant (∼0.31) above 830 °C.

Figure 12 shows the Arrhenius plot of the oxygen permeation flux through the SBFM membrane. For comparison, the oxygen permeabilities of $BaCe_{0.15}Fe_{0.85}O_{3-\delta}$ (BCF) and $La_{0.6}Sr_{0.4}Co_{0.2}Fe_{0.8}O_{3-\delta}$ (LSCF) membranes were also measured under identical experimental conditions. These membranes were prepared by the same experimental method and process as that of the SBFM membrane, and their structure and chemical properties can be found in the literature.[11,40] The thickness of each membrane was 1.0 mm. The oxygen permeation fluxes of these membranes increased monotonously with increasing the temperature. At 900 °C, the oxygen permeation flux of SBFM membrane was 4.39 × 10^{-7} mol cm^{-2} s^{-1}, which was similar to that of the BCF membrane and higher than that of LSCF membranes. The oxygen permeation flux of 1.80 × 10^{-7} mol cm^{-2} s^{-1} was obtained for the SBFM membrane at 700 °C, which was close to that of the LSCF membrane at 900 °C. Moreover, the activation energy (E_a) of oxygen permeation through the SBFM membrane was 42 kJ mol^{-1}, which was significantly lower than that of the BCF and LSCF membranes. This suggests that the SBFM membrane was suitable to separate oxygen in the intermediate temperature (600−800 °C). It is noted that the oxygen permeation flux of the SBFM membrane could be further improved by the preparation of an asymmetric membrane with a thin membrane layer and a porous support layer.[41,42]

4. Conclusions

A new $Sr_{0.7}Ba_{0.3}Fe_{0.9}Mo_{0.1}O_{3-\delta}$ (SBFM) cubic perovskite oxide was reported as an oxygen-permeable material. This material presented a high reduction-tolerant property and relatively high thermal stability. The high chemical stability of SBFM in a reducing environment was associated with the possible synergistic effect between Mo ion and Fe ion. In addition, SBFM membrane exhibited good oxygen permeability and low oxygen permeation activation energy. The remarkable performances demonstrated that SBFM could be used as an attractive oxygen-permeable material for catalytic membrane reactors. In addition, this work

(40) Li, S. G.; Jin, W. Q.; Huang, P.; Xu, N. P.; Shi, J.; Lin, Y. S. *J. Membr. Sci.* **2000**, *166*, 51.
(41) Chang, X. F.; Zhang, C.; Jin, W. Q.; Xu, N. P. *J. Membr. Sci.* **2006**, *285*, 232.
(42) Watanabe, K.; Yuasa, M.; Kida, T.; Shimanoe, K.; Teraoka, Y.; Yamazoe, N. *Chem. Mater.* **2008**, *20*, 6965.

indicates that it is possible to break the trade-off between the oxygen permeability and stability of MIEC oxide.

Acknowledgment. The authors sincerely thank Prof. Yihua Ma (Worcester Polytechnic Institute, USA) for his helpful discussions. This work is supported by the National Basic Research Program of China (No. 2009CB623406); National Natural Science Foundation of China (No. 20990222); "Six kinds of important talents" program of Jiang Su (2007007); China Postdoctoral Science Foundation funded project (Nos. 20090461105 and 200902138).

Supporting Information Available: The details of iodometric titration experiment; ICP-OES results; XPS peak fitting parameters; element valence composition of SBFM oxide; and the thermal expansion behaviors of SBFM (PDF). This material is available free of charge via the Internet at http://pubs.acs.org.